University of Aden Journal of Natural and Applied Sciences., vol.29(2) (2025) 37-45

University of Aden Journal of Natural and Applied Sciences

Journal homepage: https://uajnas.adenuniv.com

Research Article

Integrated Assessment of Natural Radioactivity and Trace-Metal Enrichment in Lahj Soils Using HPGe, ICP-MS, and XRF

Shaif Mohammed Kasem Saleh*[1]; Saleh Al-Turki[2]; Emran Eisa Saleh[1]

[1]Department of Chemistry, Faculty of Science, University of Aden, Aden, -Yemen

[2]Department of Chemistry, Saber Faculty of Applied and Human Sciences - University of Lahj, Yemen.

https://doi.org/10.47372/uajnas.2025.n2.a04

ARTICLE INFO

Received: 13/12/2025

Accepted: 29/3/2026

Keywords:

Natural radionuclides, HPGe, ICP-MS, XRF, Environmental monitoring, Soil contamination, Geochemistry.

Abstract

This study reports the activity concentrations of 40K, 232Th, and 226Ra for 21 surface soil samples from Lahj Governorate, Yemen, with mean values of 714.5 Bq/kg, 30.7 Bq/kg, and 28.2 Bq/kg, respectively. Major-oxide analyses by XRF revealed SiO_2 contents between 60.5 % and 71.8 % and K_2O between 1.46 % and 3.23 %, and a near-perfect correlation (r = 0.99) was found between K_2O and 40K activity, confirming K-bearing minerals as primary hosts for 40K. Trace-oxide data (Cr_2O_3: 0.024–0.078 %, V_2O_5: 0.010–0.043 %, MnO: 0.051–0.169 %) were strongly associated with ICP-MS metal concentrations (Cr up to 776 ppm, V up to 431 ppm, Mn up to 1 127 ppm), indicating shared mineral phases. Integrating HPGe, ICP-MS, and XRF techniques provides a cohesive multi-method framework for assessing natural radioactivity and heavy-metal distributions in under-studied soils.

1. Introduction

Environmental contamination by naturally occurring radionuclides and heavy metals poses a persistent concern for ecological and public health, particularly in regions with unique geological features or anthropogenic influences. Accurate assessment of such contaminants is essential for identifying potential hazards, evaluating exposure levels, and supporting effective mitigation strategies. Over the years, a variety of analytical techniques have been developed to quantify both radioactive elements and heavy metals in environmental matrices such as soil and water. Among the most commonly used techniques are gamma-ray spectrometry using High-Purity Germanium (HPGe) detectors, Inductively Coupled Plasma Mass Spectrometry (ICP-MS), and X-ray Fluorescence (XRF) spectrometry. Each of these methods offers specific advantages in terms of sensitivity, elemental specificity, and sample preparation requirements [1-4].

HPGe detectors, typically employed in gamma spectrometry, are highly effective for identifying and quantifying gamma-emitting radionuclides such as potassium-40 (^{40}K), uranium-series (^{226}Ra), and thorium-series (^{232}Th) isotopes. The strength of this method lies in its ability to directly measure activity concentrations (in Bq/kg) without extensive sample digestion, making it ideal for assessing natural radioactivity in solid matrices. However, it does not provide information on non-radioactive heavy metals or stable isotopes of radioactive elements [5-7].

ICP-MS, on the other hand, is a powerful technique that allows for the precise quantification of trace elements and heavy metals at extremely low concentrations, often down to parts per billion (ppb) or lower. By ionizing the sample using a high-temperature plasma and measuring the resulting ions by their mass-to-charge ratio, ICP-MS offers excellent sensitivity and is particularly suitable for detecting transition metals, rare earth elements, and actinides. Nevertheless, its reliance on wet digestion and the complexity of sample preparation can be limiting factors in large-scale environmental assessments [8-10].

X-ray Fluorescence (XRF) spectrometry provides a non-destructive, rapid, and cost-effective means of analyzing the elemental composition of samples, especially oxides of metals and metalloids in soil. It determines the concentration of elements by detecting the secondary (fluorescent) X-rays emitted from a sample when it is excited by a primary X-ray source. While XRF cannot directly measure activity concentrations or isotopic ratios, it yields the oxide forms of elements such as K_2O, ThO_2, and U_3O_8. These oxide concentrations can be converted into elemental forms and

* Correspondence to: University of Aden- Yemen

E-mail address: Shaifm2002@gmail.comt

even compared with the radiometric or mass spectrometry-derived concentrations for validation and cross-calibration purposes [11].

Numerous studies have reported varying levels of natural radioactivity in soil and water across different regions of Yemen, including the Abyan and Tuban deltas and the Hifan area[12]. Groundwater and hot spring waters have shown measurable concentrations of naturally occurring radionuclides such as radium, thorium, and uranium, reflecting the geological characteristics of these areas[13]. Surface soil samples, especially those collected near industrial sites, such as the oil refinery in Aden Assoghra, exhibit elevated radioactivity levels, indicating potential contributions from both natural sources and anthropogenic activities[14] . Collectively, these findings are crucial for understanding environmental radiation hazards and for developing protective strategies regarding exposure to natural radioactivity in Yemen.

In this study, we aim to describe and compare the sample preparation procedures for each of the three analytical techniques HPGe detector, ICP-MS, and XRF by carefully analyzing a set of environmental samples using all three methods. Through this multi-technique approach, we derive and apply the appropriate conversion equations to facilitate cross-comparison of the results obtained from these different analytical platforms. This enables us to evaluate the level of agreement or discrepancy among the measurements provided by each technique, thereby assessing their consistency and reliability. By integrating these methodologies, we enhance the credibility of radioactivity and heavy metal assessments and contribute to the development of more robust and standardized environmental monitoring protocols, which are particularly crucial in under-studied and potentially vulnerable regions such as Lahj, Yemen.

2. Materials and methods:

2.1. Description of Study Areas

This study was carried out in Lahj Governorate, situated in the southwestern part of Yemen between latitudes 12°–14°N and longitudes 43°–46°E. The region is bordered by Al-Bayda, Al-Dhale, and Taiz to the north, Abyan to the east, Taiz to the west, and both the city of Aden and the Gulf of Aden to the south. Lahj extends over approximately 12,648 square kilometers and has a population exceeding 850,000, distributed across 15 districts, with Al-Hawtah serving as the administrative capital.

The governorate lies on the delta of Wadi Tuban, where extensive agricultural activity takes place due to the presence of fertile alluvial soils. These soils, enriched by seasonal sediment deposition, support the cultivation of vegetables and fodder crops and are a key component of the region's economy. The climate is typically arid to semi-arid, featuring hot summers and mild winters.

Geologically, Lahj is characterized by sedimentary formations, including clay-rich layers that influence both the physical and chemical properties of surface soils. These characteristics make the area significant for studying natural and anthropogenic influences on soil composition. Soil samples were systematically collected from different locations across the governorate, ensuring coverage of both agricultural zones and areas potentially impacted by human activities. Each sample was handled according to standard environmental sampling protocols to maintain analytical reliability.

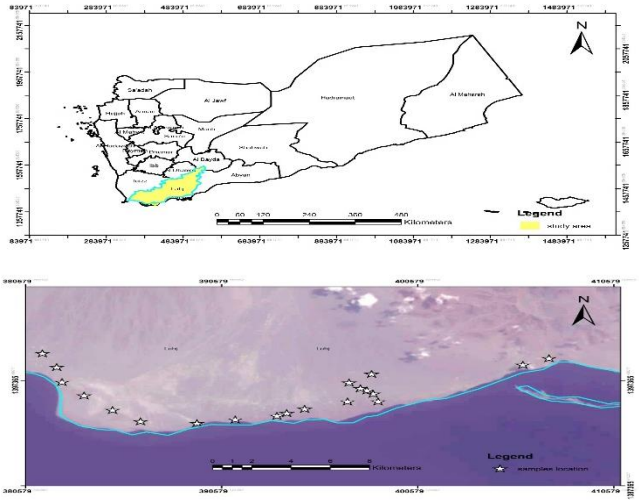

Fig1: Shows the area of the study

2.2. Sample Preparation

In this study, a total of 21 surface soil samples were systematically collected from multiple locations across Lahj Governorate, ensuring spatial representation of different environmental and land-use settings. The sampling sites were selected based on agricultural activity, proximity to potential anthropogenic sources, and geological variability. Each soil sample was taken from the top 0–7 cm layer to reflect recent environmental conditions and human influences. Approximately 700–1200 grams of soil were collected at each location using clean plastic tools to avoid cross-contamination, and the samples were placed in pre-labeled, sealed polyethylene bags.

The collected samples were immediately transported to the laboratory under dry and stable conditions. During transport, care was taken to protect the samples from moisture and extreme temperature fluctuations. Upon arrival, all samples were cataloged and stored in a designated dry area pending preparation [15, 16].

For radiological measurements using the High-Purity Germanium (HPGe) detector, the samples were first air-

dried and then oven-dried at 105 °C for 24 hours to remove all residual moisture. Once dried, the soil was homogenized and ground using a DISC MILL followed by a BALL MILL to achieve fine, uniform particle size. The powdered samples were sieved through a 2 mm mesh to remove gravel and plant debris, then packed into 65 mL cylindrical polyethylene Marinelli beakers. Each container was hermetically sealed to prevent the escape of radon gas and stored for 30 days to allow secular equilibrium between uranium, thorium, and their decay products prior to gamma spectrometric analysis.

For chemical analysis by Inductively Coupled Plasma Mass Spectrometry (ICP-MS), a representative portion of each soil sample was subjected to acid digestion. About 0.5 grams of dried and homogenized soil was weighed and transferred into Teflon digestion vessels. A mixture of high-purity analytical-grade acids, including nitric acid (HNO_3), hydrochloric acid (HCl), and hydrofluoric acid (HF), was added in accordance with the EPA 3052 method. The digestion process was performed in a microwave digestion system to ensure complete dissolution of both silicate and metallic phases. After digestion, the solutions were filtered and diluted with deionized water to a known volume. Internal standards and calibration solutions were used to ensure analytical accuracy and traceability [17, 18].

For X-ray fluorescence (XRF) spectroscopy, a separate aliquot of each sample was prepared by drying and grinding, followed by pressing into solid pellets. Approximately 5 grams of the fine powder was pressed into 32 mm diameter discs using a hydraulic press under a pressure of 20 tons. The pressed pellets were labeled and stored in desiccators until measurement. Prior to analysis, the XRF spectrometer was calibrated using certified reference materials to ensure accurate elemental quantification [19].

This multi-technique preparation and analysis protocol ensures high data quality, allowing for comparative evaluation of elemental concentrations and radiological activity in the studied soil samples.

3. Analytical Methods

To determine the concentrations of naturally occurring radionuclides and major and trace elements in the collected soil samples, three analytical techniques were employed: gamma-ray spectrometry using a HPGe detector, ICP-MS, and XRF. Each method was chosen for its sensitivity, selectivity, and suitability for the targeted analytes.

Gamma-ray Spectrometry (HPGe)

A high-purity germanium (HPGe) detector system with 40% relative efficiency and a full width at half maximum (FWHM) resolution of 2.0 keV at 1.33 MeV (^{60}Co) was utilized to measure gamma-emitting radionuclides in the soil samples. To minimize background radiation and improve detection sensitivity, the detector was housed in a 10 cm-thick lead shield, lined internally with 1 mm of aluminum and 1.6 mm of copper. The entire assembly was placed in a low-background room with 1 m-thick concrete walls additionally lined with 3 mm lead sheets.

Energy and efficiency calibrations were performed using a mixed gamma standard source provided by the Czech Metrological Institute (CMI), which includes 11 radionuclides with energies ranging from 60 keV to 1836 keV. The calibration standard had a geometry and matrix closely matching that of the soil samples. Sample spectra were acquired over a counting time of 60,000 seconds to ensure reliable detection of low-activity radionuclides. The Genie 2000 software was employed for spectral analysis, including energy calibration, peak identification, efficiency correction, activity calculation, background subtraction, uncertainty estimation, and minimum detectable activity (MDA) determination. The activity of each radionuclide was calculated using the standard formula [20, 21]:

$$A(BqKg^{-1}) = \frac{C}{\varepsilon YMT} \qquad (1)$$

In this formula, C represents the total area under the spectral peak, ε denotes the detector's efficiency specific to the energy of the γ-ray, Y indicates the intensity of the γ-ray emissions, M symbolizes the mass of the sample in kg, and T signifies the duration of the collection period in seconds.

Inductively Coupled Plasma Mass Spectrometry (ICP-MS)

For trace metal analysis, soil samples were digested using a combination of high-purity HNO_3, HCl, and HF acids in closed Teflon vessels following the microwave-assisted EPA 3052 method. The digested solutions were filtered and diluted appropriately before analysis.

The ICP-MS system was operated under standard plasma conditions: RF power of 1550 W, argon gas flow rates of 15 L/min (coolant), 1.0 L/min (auxiliary), and 1.1 L/min (nebulizer). Internal standards such as indium (^{115}In) and rhodium (^{103}Rh) were used to correct for instrumental drift and matrix effects. Calibration curves were established using certified multi-element standard solutions.

The instrument's detection limits (LOD) for most elements were in the range of sub-ppb, depending on the analyte and matrix complexity. Collision/reaction cell technology was employed to minimize polyatomic interferences and improve the accuracy of measurements, especially for elements such as As, Se, and Cr [22, 23].

X-ray Fluorescence Spectrometry (XRF)

Major oxides and some trace elements were quantified using XRF analysis. The instrument used was a wavelength-dispersive XRF spectrometer operating at a voltage of 50 kV and current of 50 mA. Soil samples were pressed into 32 mm diameter pellets under a pressure of 20 tons without the use of a binding agent to avoid contamination.

Prior to measurement, the instrument was calibrated using a suite of certified reference materials (CRMs) that closely matched the matrix of the soil samples.

The XRF technique offered reliable detection of oxides such as SiO_2, Al_2O_3, Fe_2O_3, CaO, MgO, Na_2O, K_2O, and TiO_2. The method detection limits (MDL) for major oxides typically ranged from 0.01% to 0.05%, depending on the element and matrix composition. Quality assurance was maintained through repeated measurements of CRMs and blanks, ensuring the analytical accuracy and reproducibility of the results [24, 25]

4. Conversion Equations

To ensure the comparability and integration of results obtained from different analytical techniques (HPGe, ICP-MS, and XRF), several conversion equations were employed. These equations facilitate the transformation of measurement units and formats, allowing for consistent interpretation across radiological and chemical data domains[26-29].

1. Conversion of Radioactivity (Bq/kg) to Elemental Concentration (ppm or mol/kg)

For gamma spectrometry results, the activity concentration A (in Bq/kg) of a radionuclide can be converted to the corresponding elemental concentration using the following relation:

$$C_{mol} = \frac{A}{\lambda N_A} \qquad (2)$$

Where: C_{mol} is the molar concentration (mol/kg), A is the activity concentration (Bq/kg), $\lambda = \frac{ln\,2}{T_{1/2}}$ is the decay constant (s^{-1}), N_A = 6.022×10^{23} Avogadro's number mol^{-1}, and $T_{1/2}$ is the half-life of the radionuclide (s).

To express the result in *parts per million (ppm)*, the following transformation is applied:

$$C_{ppm} = C_{mol}\, M_r \,.\, 10^3 \qquad (3)$$

Where M_r is the molar mass of the element (g/mol). This dual conversion allows for direct comparison between radiological and chemical concentrations, especially when assessing elements such as uranium or thorium, which are reported in both domains.

2. Conversion of XRF Oxide Percentages to Elemental Concentrations

XRF analysis often reports results in terms of metal oxides (e.g., U_3O_8, ThO_2, Fe_2O_3, etc.). To compare these results with elemental concentrations from ICP-MS or decay-based estimates, it is necessary to convert oxide mass percentages into pure elemental concentrations using the molecular weight ratios.

The general equation is:

$$C_{element} = C_{oxide} \cdot \frac{M_{element}}{M_{oxide}} \qquad (4)$$

Where $C_{element}$ is the concentration of the element (wt%), C_{oxide} is the concentration of the oxide (wt%), $M_{element}$ is the molar mass of the element (e.g., Fe = 55.85 g/mol), and M_{oxide} is the molar mass of the corresponding oxide (e.g., Fe_2O_3 = 159.7 g/mol).

3. Harmonization of Molar Concentrations from Gamma Spectrometry with ICP-MS Results

Since ICP-MS typically provides elemental concentrations in *ppb or ppm (µg/kg or mg/kg)*, and HPGe-derived concentrations are calculated in *mol/kg*, harmonization requires transforming molar values into mass-based units:

$$C_{mg/kg} = C_{mol/kg}\, M_r \,.\, 10^3 \qquad (5)$$

Where: $C_{mg/kg}$ is the concentration in mg/kg (or ppm), $C_{mol/kg}$ is the molar concentration, and M_r is the molar mass (g/mol).

This conversion is particularly useful when comparing the estimated elemental content from radioactive decay with that measured directly via mass spectrometry.

90%) at pH 9 and (Ni – Gly2) at pH 7 (ca . 70%). The major species (Ni – Gly) is obtained by deprotonation of the amino and carboxylate groups formation begins at pH 6 (ca – 60%). Zinc (II) forms two complexes with Glycine, the species distribution is shown in Fig (11b), The formation of complex (Zn – Gly) is started at pH 3.3 and its Maximum Concentration was ca.50 % at pH 5 and (Zn – Gly_2) at pH 7 ca. 90 %. The interaction of Cadmium (II) and Glycine are shown in Fig (11c) formed three Complexes. The Complex (Cd – Gly) is formed at pH 3.5 and its maximum concentration was ca.55 % at pH 6 and Cd-Gly_2 formed at pH 6 , and its maximum concentration ca. 30% at pH 7.5 . The various El device allows the quantitative determination of the carbon, nitrogen and hydrogen in various operating modes. For the synthesized, Nickel, zinc and cadmium Complexes. The Data of the elemental analysis for metal ion amino acids complexes are illustrated in Table (5).

5. Results and Discussion

Prior to examining the mineralogical controls on radionuclide behavior, the basic radiological and geochemical data are summarized in Tables 1 and 2. Table 1 lists the activity concentrations of ^{226}Ra, ^{232}Th, and ^{40}K in each soil sample as determined by HPGe gamma spectrometry. Table 2 reports the corresponding oxide percentages and trace–oxide levels measured by XRF. Together, these two datasets establish both the radiological baseline and the geochemical framework.

Table 1: Concentration of radioactive activity for 226Ra, 232Th and 40 K in Soil samples.

Sample NO.	Activity concentration (Bq kg^{-1})		
	^{40}K	^{232}Th	^{226}R
S1	734.8±29.3	34.4±2.6	33.5±1.5
S2	953.0±31.1	30.3±2.3	34.3±1.5
S3	642.3±26.4	20.3±1.9	21.5±1.3
S4	990.3±35.3	43.6±2.9	67.9±1.7
S5	448.8±21.5	18.4±1.9	14.5±1.2
S6	763.7±27.4	25.6±2.1	31.7±1.0
S7	831.2±29.4	33.1±2.3	29±1.4
S8	540.3±23.2	16.3±1.8	17±1.1
S9	499.9±23.2	21.4±1.9	22.7±1.3
S10	861.6±30.4	33.1±2.7	29.6±1.5
S11	460.5±22.7	21.7±1.8	21.7±1.3
S12	937.6±32.9	41.5±2.8	40±1.7
S13	459.8±20.1	18.2±1.7	14.5±0.9
S14	476.3±20.6	19.9±1.8	23.3±0.9
S15	871.4±34.6	39.9±2.9	36.5±1.8
S16	790.9±33.6	28.5±2.6	35.2±1.3
S17	877.0±33.3	36.4±2.9	13.8±1.7
S18	961.9±33.1	93.3±2.7	33.3±1.6
S19	906.5±29.9	34.5±2.4	29.5±1.4
S20	513.7±23.4	18.5±2.1	24.7±1.4
S21	482.9±23.2	15.9±1.8	17.1±1.2
Range	**448.8-990.3**	**15.9-93.3**	**13.8-67.9**
Average	**714.50**	**30.70**	**28.16**

The X-ray fluorescence (XRF) analysis offered comprehensive insights into the geochemical composition of the collected soil and rock samples, particularly in explaining the patterns of natural radioactivity and heavy metal distribution. Table 3 presents the major oxide concentrations derived from XRF alongside the activity concentrations of radionuclides (^{40}K, ^{226}Ra, ^{232}Th) obtained via HPGe gamma spectrometry. As illustrated in the table, samples exhibiting higher percentages of K_2O (e.g., S4 and S12) also show elevated levels of ^{40}K activity, suggesting a strong geochemical coupling between potassium-bearing minerals (such as K-feldspars and biotite) and the presence of ^{40}K.

To statistically assess the relationships between major oxide components and radionuclide activity levels, Figure 2, presents the Pearson correlation matrix calculated between SiO_2, Al_2O_3, Fe_2O_3, K_2O, and the radionuclides ^{40}K, ^{226}Ra, and ^{232}Th. The analysis reveals a remarkably strong positive correlation between K_2O and ^{40}K ($r = 0.99$), highlighting the mineralogical link between potassium-rich phases (e.g.,

feldspars and micas) and the presence of naturally occurring potassium-40. Additionally, moderate to strong correlations are observed between K_2O and both ^{226}Ra ($r = 0.67$) and ^{232}Th ($r = 0.69$), suggesting that potassium-bearing minerals may also influence the mobility or retention of uranium- and thorium-series radionuclides. In contrast, SiO_2 shows negligible correlations with all radionuclides, implying a limited geochemical influence of silica on radionuclide distribution despite its dominance in the mineral matrix.

The XRF results reveal notable enrichments in trace oxides–Cr_2O_3, V_2O_5, and MnO–across the 21 soil samples, with Cr_2O_3 ranging from 0.0241% to 0.0776%, V_2O_5 from 0.0103% to 0.0431%, and MnO from 0.0509% to 0.1686%. Table 3 couples these oxide abundances with their corresponding element concentrations–chromium (Cr), vanadium (V), and manganese (Mn)–now derived via ICP-MS (Cr, V) or stoichiometric conversion (Mn). A clear geochemical affinity emerges: Sample S18, with the highest Cr_2O_3 (0.0776%), also shows the greatest Cr content (776 ppm), indicating strong Cr-rich mineral phases. Vanadium mirrors this pattern in Sample S20, where V_2O_5 reaches 0.0431% alongside the highest V concentration of 431 ppm. Manganese follows suit, peaking in Sample S10 (MnO 0.1456%) with 1,127 ppm Mn, underscoring MnO's reliability as a proxy for Mn enrichment. These consistent element-oxide pairings suggest shared mineral hosts–such as chromite for Cr, vanadates for V, and pyrolusite or braunite for Mn–and provide a robust basis for mapping trace-metal distributions in Lahj soils.

Table 2: Major and Trace Oxide Composition of Lahij Soil Samples Determined by XRF

Sample NO.	Al_2O_3 (%)	CaO (%)	Fe_2O_3 (%)	K_2O (%)	MgO (%)	P_2O_5 (%)	SiO_2 (%)	TiO_2 (%)	Cr_2O_3 (PPM)	MnO (PPM)	Na_2O (%)	SrO (PPM)	V_2O_5 (PPM)
S1	12.53	4.65	6.11	2.52	1.96	0.15	62.68	1.38	291	1,495	3.28	536	318
S2	11.50	3.88	5.10	3.16	1.37	0.18	64.90	1.00	324	1,291	3.66	499	214
S3	8.82	10.83	2.68	2.12	1.14	0.23	60.51	0.53	307	509	2.78	1,063	103
S4	12.09	2.98	4.29	3.21	1.21	0.13	68.19	0.82	336	1,027	3.46	410	196
S5	11.15	5.96	6.49	1.46	2.69	0.24	62.59	1.53	269	1,222	2.52	540	415
S6	10.43	7.25	4.12	2.59	1.48	0.17	62.98	0.85	285	984	3.20	718	186
S7	11.63	5.33	4.86	2.75	1.75	0.18	63.89	1.04	253	1,191	3.24	584	237
S8	11.15	4.87	5.85	1.73	2.09	0.19	65.80	1.34	302	1,099	3.09	542	347
S9	11.27	5.28	6.69	1.73	2.55	0.24	63.75	1.51	291	1,314	2.86	520	384
S10	11.64	4.73	5.66	2.74	1.73	0.19	62.36	1.20	513	1,456	3.81	576	277
S11	11.17	6.06	6.61	1.47	2.72	0.24	61.45	1.54	424	1,222	2.57	515	379
S12	12.58	3.12	4.74	3.12	1.31	0.14	66.65	0.92	360	1,237	3.51	449	175
S13	9.90	4.96	5.65	1.55	1.98	0.20	67.51	1.26	241	1,167	3.13	521	341
S14	10.43	5.15	5.90	1.57	2.06	0.21	71.80	1.32	255	1,242	3.28	542	324
S15	12.06	3.85	5.23	3.01	1.61	0.15	65.13	1.10	573	1,340	3.48	495	236
S16	10.66	7.11	4.72	2.69	1.60	0.17	62.31	0.96	415	1,162	3.16	709	206
S17	11.96	4.28	5.50	2.94	1.78	0.16	64.08	1.19	569	1,367	3.61	512	247
S18	11.37	4.29	5.32	3.19	1.44	0.19	64.07	1.06	776	1,338	3.74	523	235
S19	11.44	4.28	4.97	3.23	1.38	0.19	64.51	1.02	329	1,288	3.64	533	209
S20	10.53	5.19	7.29	1.63	2.51	0.24	64.29	1.66	371	1,424	2.81	492	431
S21	10.77	5.17	6.15	1.70	2.09	0.19	65.38	1.37	464	1,175	3.32	577	341

Table 3: Major Oxide Composition (%) from XRF Analysis and Corresponding Radioactive Nuclide Activities

Sample ID	SiO_2 (%)	Al_2O_3 (%)	Fe_2O_3 (%)	K_2O (%)	^{40}K (Bq/kg)	^{226}Ra (Bq/kg)	^{232}Th (Bq/kg)
S4	68.19	12.09	4.29	3.21	990	68	43.6
S8	65.8	11.15	5.85	1.73	540	17	16.3
S12	66.65	12.58	4.74	3.12	938	40	41.5
S13	67.51	9.9	5.65	1.51	460	14.5	19.9
S14	71.8	10.43	5.9	1.57	476	23.3	18.2
S21	65.38	10.77	6.15	1.7	483	17.1	16

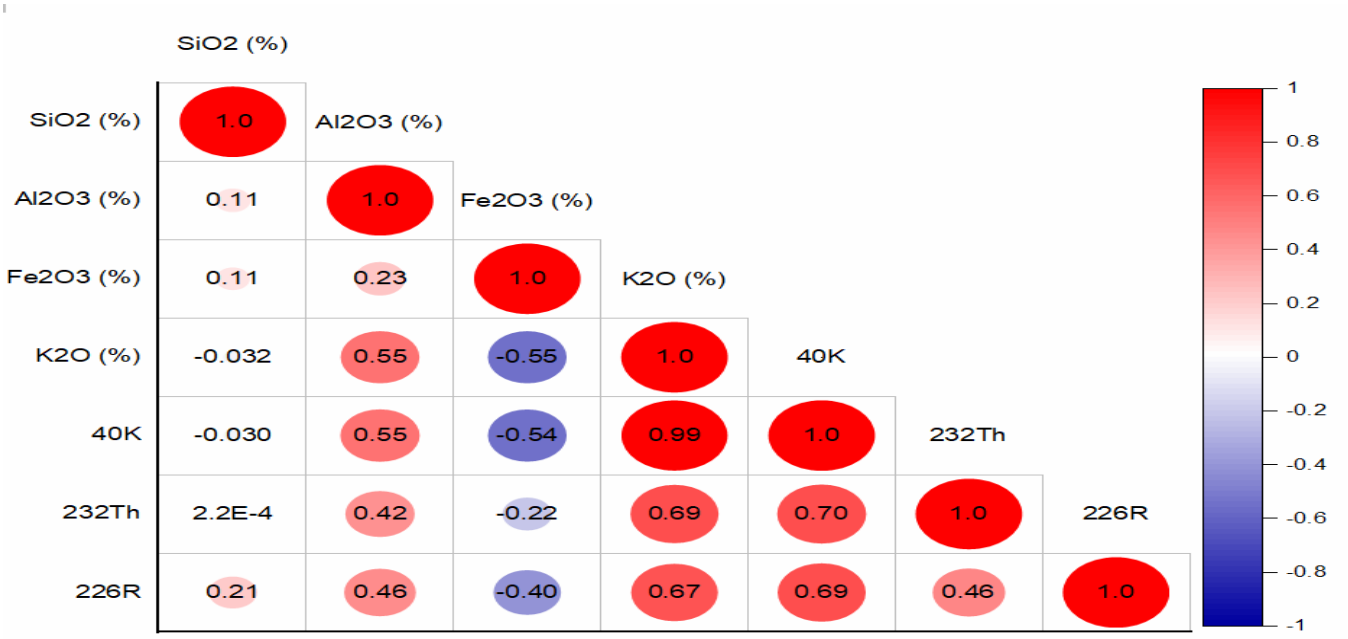

Figure 1: Correlation Matrix between Major Oxide Components and Natural Radionuclide Activities in Soil

Taken together, these results demonstrate a high degree of consistency and complementarity between XRF, HPGe gamma spectrometry, and ICP-MS analyses. The chemical composition of the soils–particularly the abundances of potassium, aluminum, iron, and titanium oxides–directly governs the spatial variability of natural radioactivity and heavy-metal concentrations, with silicate-rich matrices and alumino-ferric or phosphate-bearing minerals acting as effective sinks for both radionuclides and toxic elements. Each technique brings its own strengths and limitations: HPGe excels at rapid in-situ surveys of gamma-emitting radionuclides yet is sensitive to counting statistics, calibration drift, and equilibrium delays; ICP-MS provides ultra-trace elemental and isotopic analyses but depends on complete digestion and is subject to spectral interferences; and XRF enables fast, high-resolution screening of major and some trace oxides, though accuracy hinges on pellet homogeneity and detection limits. By cross-validating activity concentrations with elemental and oxide abundances, we mitigate method-specific biases and establish a robust multi-technique protocol for environmental radioactivity and heavy-metal assessment in under-studied regions such as Lahj, Yemen.

Conclusion

The soils of Lahj exhibit a moderate natural radiological background, with mean activity concentrations of 714.5 Bq/kg for ^{40}K, 30.7 Bq/kg for ^{232}Th, and 28.2 Bq/kg for ^{226}Ra. Geochemical analysis reveals that potassium-bearing minerals–principally K-feldspars and micas–play a dominant role in hosting ^{40}K, as demonstrated by an almost perfect correlation ($r = 0.99$) between K_2O content (1.46–3.23 %) and ^{40}K activity. In addition, iron- and aluminum-oxide phases show moderate correlations ($r \approx 0.67$) with ^{226}Ra and ^{232}Th, underscoring the importance of alumino-ferric silicates in radionuclide retention. Trace-oxide abundances determined by XRF–Cr_2O_3 up to 0.0776 %, V_2O_5 up to 0.0431 %, and MnO up to 0.1686 %–align closely with ICP-MS–measured metal contents of Cr (776 ppm), V (431 ppm), and Mn (1 127 ppm), confirming that oxide proxies reliably predict heavy-metal enrichment. Together, these multi-technique findings establish a robust protocol for integrated radioactivity and heavy-metal screening in arid agricultural soils and provide a solid foundation for targeted risk-mitigation strategies in Lahij, Yemen.

Acknowledgments

The authors gratefully acknowledge the Department of Chemistry, University of Aden for providing instrumental facility.

Disclosure

The authors should clear the conflicts of interest in their work.

6. References

1. Wei-Xin, L., et al., *A comparative analysis of environmental quality assessment methods for heavy metal-contaminated soils.* Pedosphere, 2008. **18**(3): p. 344-352.
2. Suciu, I., et al., *Analysis of soil heavy metal pollution and pattern in Central Transylvania.* International journal of molecular sciences, 2008. **9**(4): p. 434-453.
3. Zhiyuan, W., et al., *Assessment of soil heavy metal pollution with principal component analysis and geoaccumulation index.* Procedia Environmental Sciences, 2011. **10**: p. 1946-1952.
4. Gupta, N., et al., *Analyzing contamination of heavy metals—ICP-MS and SEM-EDS*, in *Heavy Metals in the Environment: Management Strategies for Global Pollution*. 2023, ACS Publications. p. 205-225.
5. Kurup, P., et al., *A review of technologies for characterization of heavy metal contaminants.* Indian Geotechnical Journal, 2017. **47**: p. 421-436.
6. Maglas, N.N., et al., *Assessment of radioactive nuclides and heavy metals in soil and drink water in Lahij city, Yemen.* Applied Radiation and Isotopes, 2025. **215**: p.
7. Wang, Z., et al., *Overview assessment of risk evaluation and treatment technologies for heavy metal pollution of water and soil.* Journal of Cleaner Production, 2022. **379**:
8. Beauchemin, D., *Inductively coupled plasma mass spectrometry.* Analytical chemistry, 2008. **80**(12): p. 4455-4486.
9. Olesik, J.W., *Elemental analysis using icp-oes and icp/ms.* Analytical Chemistry, 1991. **63**(1): p. 12A-21A.
10. Ashrit, S., et al., *Application of ICP-MS technique for analysis of heavy metals in LD slag fines.* Current Science, 2018. **115**(5): p. 973-977.
11. Borges, C., et al., *Comparison of portable X-ray fluorescence spectrometry and laboratory-based methods to assess the soil elemental composition: Applications for wetland soils.* Environmental Technology and Innovation, 2020. **19**: p. 100826.
12. Saleh, E., et al., *Enhancement of natural radioactivity in farm surface soils from Abyan Delta in Yemen.* International Journal of Low Radiation, 2015. **10**: p. 34-
13. El-Mageed, A., et al., *Natural radioactivity of ground and hot spring water in some areas in Yemen.* Desalination, 2013. **321**: p. 28–31.
14. Abdullah, M.G. and E.E. Saleh, *Assessment of natural and anthropogenic radioactivity levels and their radiological hazards in surface soil samples around oil refinery, Aden Assoghra city, Yemen.* University of Aden Journal of Natural and Applied Sciences, 2023. **27**(2): p.
15. Alsafadi, K., et al., *An integration of bioclimatic, soil, and topographic indicators for viticulture suitability using multi-criteria evaluation: a case study in the Western slopes of Jabal Al Arab—Syria.* Geocarto International, 2020. **35**(13): p. 1466-1488.
16. El-Zeiny, A.M. and H.A. Effat, *Environmental analysis of soil characteristics in El-Fayoum Governorate using geomatics approach.* Environmental monitoring and assessment, 2019. **191**: p. 1-20.
17. Zhong, C., et al., *Effect of water content in soil samples on the {gamma} detection efficiency for HPGe {gamma} spectrometer.* Nuclear Electronics and Detection Technology, 2005. **25**.
18. Benke, R. and K. Kearfott, *Soil sample moisture content as a function of time during oven drying for gamma-ray spectroscopic measurements.* Nuclear Instruments and Methods in Physics Research Section A: Accelerators, Spectrometers, Detectors and Associated Equipment, 1999. **422**(1-3): p. 817-819.
19. Sverchkov, I., et al., *Method of reference samples preparation for X-ray fluorescence analysis.* Talanta, 2023. **252**: p. 123820.
20. Joel, G.S.C., et al., *Precision measurement of radioactivity in gamma-rays spectrometry using two HPGe detectors (BEGe-6530 and GC0818-7600SL models) comparison techniques: application to the soil measurement.* MethodsX, 2017. **4**: p. 42-54.
21. Thakur, S., et al., *Spectroscopic performance evaluation and modeling of a low background HPGe detector using GEANT4.* Nuclear Instruments and Methods in Physics Research Section a: Accelerators, Spectrometers, Detectors and Associated Equipment, 2024. **1058**: p.
22. Dlamini, H., P. Mahlambi, and S. Mngadi, *Validation of microwave-assisted digestion and Inductive coupled plasma-mass spectrometer for the determination of trace metals in the soil around Darvill sludgeland and their environmental complications.* Soil and Sediment Contamination: An International Journal, 2023. **32**(6): p. 637-651.
23. Schmidt, K., D. Autenrieth, and R. Nagisetty, *A comparison of field portable X-ray fluorescence (FP XRF) and inductively coupled plasma mass spectrometry (ICP-MS) for analysis of metals in the soil and ambient air.* Research square, 2024: p. rs. 3. rs-3849271.
24. Shrestha, G., et al., *Quantification of multiple soil trace elements by combining portable X-ray fluorescence and reflectance spectroscopy.* Geoderma, 2022. **409**: p.
25. Vivit, D.V. and B.S.W. KING, *The determination of major oxide and trace element concentrations in eighteen Chinese standard reference samples by X-ray fluorescence spectrometry.* Geostandards Newsletter, 1988. **12**(2): p. 363-370.
26. Choppin, G., et al., *Radiochemistry and nuclear chemistry*. 2013: Academic Press.
27. Knoll, G.F., *Radiation detection and measurement*. 2010: John Wiley & Sons.
28. Skoog, D.A., et al., *Fundamentals of analytical chemistry*. Vol. 33. 1996: Saunders College Pub. Fort Worth.
29. Carter, S., et al., *Atomic spectrometry update: Review of advances in the analysis of metals, chemicals and materials.* Journal of Analytical Atomic Spectrometry, 2020. **35**(11): p. 2410-2474.

University of Aden Journal of Natural and Applied Sciences., vol.29(2) (2025) 37-45

مجلة جامعة عدن للعلوم الطبيعية والتطبيقية

Journal homepage: https://uajnas.adenuniv.com

بحث علمي

التقييم المتكامل للنشاط الإشعاعي الطبيعي وإثراء العناصر النزرة في تربة محافظة لحج باستخدام تقنيات HPGe و ICP-MS و XRF

شائف محمد قاسم*[1]، صالح التركي[2] ،عمران عيسى صالح[1]
قسم الكيمياء - كلية العلوم, جامعة عدن [1]
قسم الكيمياء ، كلية صبر للعلوم التطبيقية والانسانية ، جامعة لحج ، اليمن[2]

https://doi.org/10.47372/uajnas.2024.n2.a04

الملخص

تتناول هذه الدراسة قياس تراكيز النشاط الإشعاعي للنظائر الطبيعية (^226Ra، ^232Th، 40K) في 21 عينة من التربة السطحية من محافظة لحج – اليمن، حيث بلغت القيم المتوسطة 714.5 و30.7 و28.2 بيكريل/كغم على التوالي. أظهرت تحاليل الأكاسيد الرئيسية باستخدام تقنية XRF أن نسبة SiO_2 تراوحت بين 60.5% و71.8%، بينما تراوحت نسبة K_2O بين 1.46% و3.23%. كما تم تسجيل ارتباط قوي جدًا (r = 0.99) بين K_2O ونشاط ^40K، مما يؤكد أن المعادن الحاملة للبوتاسيوم تمثل المصدر الرئيسي لهذا النظير.

أظهرت بيانات الأكاسيد النزرة (مثل Cr_2O_3 وV_2O_5 وMnO) ارتباطًا وثيقًا مع تراكيز العناصر المقاسة بتقنية ICP-MS (حيث بلغ الكروم حتى 776 جزء بالمليون، والفاناديوم حتى 431 جزء بالمليون، والمنغنيز حتى 1127 جزء بالمليون)، مما يشير إلى وجود أطوار معدنية مشتركة. توضح الدراسة أن دمج تقنيات HPGe وICP-MS وXRF يوفر إطارًا تحليليًا متكاملًا لتقييم النشاط الإشعاعي الطبيعي وتوزيع المعادن الثقيلة في التربة، خاصة في المناطق التي لم تُدرس بشكل كافٍ.

مفاتيح البحث

التسليم : 13/12/2025

القبول : 29/3/2026

كلمات مفتاحية :

االنشاط الإشعاعي
:المعادن الثقيلة
،الأكاسيد النزرة